

## Article

## Atomically Dispersed Co Catalyst for Efficient Hydrodeoxygenation of Lignin-derived Species and Hydrogenation of Nitro-aromatics

Longkang Zhang, Ningzhao Shang, Shutao Gao, Junmin Wang, Tao Meng, Congcong Du, Tongde Shen, Jianyu Huang, Qiuhua Wu, Hai-Jun Wang, Yuqing Qiao, Chun Wang, Yongjun Gao, and Zhi Wang

*ACS Catal.*, **Just Accepted Manuscript** • DOI: 10.1021/acscatal.0c00239 • Publication Date (Web): 10 Jul 2020

Downloaded from [pubs.acs.org](https://pubs.acs.org) on July 10, 2020

### Just Accepted

“Just Accepted” manuscripts have been peer-reviewed and accepted for publication. They are posted online prior to technical editing, formatting for publication and author proofing. The American Chemical Society provides “Just Accepted” as a service to the research community to expedite the dissemination of scientific material as soon as possible after acceptance. “Just Accepted” manuscripts appear in full in PDF format accompanied by an HTML abstract. “Just Accepted” manuscripts have been fully peer reviewed, but should not be considered the official version of record. They are citable by the Digital Object Identifier (DOI®). “Just Accepted” is an optional service offered to authors. Therefore, the “Just Accepted” Web site may not include all articles that will be published in the journal. After a manuscript is technically edited and formatted, it will be removed from the “Just Accepted” Web site and published as an ASAP article. Note that technical editing may introduce minor changes to the manuscript text and/or graphics which could affect content, and all legal disclaimers and ethical guidelines that apply to the journal pertain. ACS cannot be held responsible for errors or consequences arising from the use of information contained in these “Just Accepted” manuscripts.

1  
2  
3  
4  
5  
6  
7  
8 **Atomically Dispersed Co Catalyst for Efficient Hydrodeoxygenation of**  
9  
10 **Lignin-derived Species and Hydrogenation of Nitro-aromatics**  
11  
12  
13  
14

15 Longkang Zhang, <sup>a†</sup> Ningzhao Shang, <sup>a†</sup> Shutao Gao, <sup>a†\*</sup> Junmin Wang, <sup>a</sup> Tao Meng, <sup>a</sup> Congcong  
16 Du, <sup>c</sup> Tongde Shen, <sup>c</sup> Jianyu Huang, <sup>c</sup> Qihua Wu, <sup>a</sup> Haijun Wang, <sup>b</sup> Yuqing Qiao, <sup>d\*</sup> Chun Wang, <sup>a\*</sup>  
17  
18 Yongjun Gao, <sup>b\*</sup> and Zhi Wang, <sup>a</sup>  
19  
20

21  
22 <sup>a</sup> *College of Science, Hebei Agricultural University, Baoding 071001, China*  
23

24  
25 <sup>b</sup> *College of Chemical and Environmental Science, Hebei University, Baoding 071000, China*  
26

27  
28 <sup>c</sup> *Clean Nano Energy Center, State Key Laboratory of Metastable Materials Science and*  
29  
30 *Technology, Yanshan University, Qinhuangdao 066004, China*  
31

32  
33 <sup>d</sup> *College of Environmental and Chemical Engineering, Yanshan University, Qinhuangdao 066004,*  
34  
35 *China*  
36  
37  
38  
39  
40  
41  
42  
43  
44  
45  
46  
47  
48  
49  
50  
51  
52  
53  
54  
55  
56  
57  
58  
59  
60

**ABSTRACT**

Single atom catalysts (SACs) have attracted much attention due to their outstanding catalytic performance in heterogeneous catalysis. Here, we reported a template sacrificial method to fabricate atomically dispersed Co catalyst, three kinds of silica template with different microstructure (MCM-41, SBA-15 and FDU-12) were employed and the impact of pore structure of the templates on the dispersity of Co was investigated. The catalysts fabricated with different template presented different Co dispersity, leading to distinguishing catalytic performance. The optimized Co<sub>1</sub>@NC-(SBA) catalyst with atomically dispersed Co displayed outstanding catalytic activity for the hydrodeoxygenation (HDO) of lignin-derived species as well as the hydrogenation of various nitroaromatics. The reaction mechanism of HDO of vanillin was investigated by using density functional theory calculations as well.

**KEYWORDS:** *single atom Co, lignin-derived species, vanillin, nitroarenes, hydrodeoxygenation, hydrogenation, density functional theory*

## INTRODUCTION

The conversion of biomass into value-added aromatic chemicals and liquid fuels has been considered as an effective way to reduce the world dependence on fossil resources and environment pollution simultaneously.<sup>1-4</sup> Lignin, a representative example of biomass, can be transformed into phenolic compounds such as bio-oil by fast pyrolysis approach. However, the high oxygen content and unsaturated degree of the obtained products always make them undesirable due to their high viscosities, low energy density, low heating value, low chemical and thermal stability.<sup>5-6</sup> Thus, many strategies such as hydrotreating, hydrodeoxygenation (HDO), hydrocracking and steam reforming of the model species of lignin-derived bio-oil have been proposed to reduce the oxygen concentration.<sup>7-9</sup> Among them, hydrodeoxygenation is an effective bio-oil upgrading strategy and has received intensive attention.

Vanillin, a typical model substance of lignin-derived bio-oil, can be selectively converted to 2-methoxy-4-methylphenol (MMP), which has been widely used as fragrances or the intermediates of drugs.<sup>10</sup> Owing to the distinguished catalytic performance of precious metal-based catalysts, tremendous efforts have been devoted to develop high-performance noble metal catalysts such as Au,<sup>11</sup> Ru<sup>12-13</sup> and Pd<sup>14-18</sup> for the HDO of vanillin. Nevertheless, the practical applications of noble metal-based catalysts are hindered by their prohibitive cost and low reserves. In this regard, the development of highly efficient and economic catalysts for the upgrading of bio-oil is of great significance. Several non-noble metal-based catalysts have been developed for the HDO of vanillin.<sup>19-27</sup> For example, Petitjean reported that Cu-PMO can convert vanillin into MMP with 90% yield at the condition of 180 °C, 4 MPa H<sub>2</sub>, 18 h.<sup>21</sup> Although Ni/NCB-900 can also catalyze the HDO of vanillin, but the selectivity of MMP was poor under mild reaction conditions.<sup>22</sup> Jiang and co-workers developed a non-noble metal catalyst named Co/N-C-600, in which the cobalt nanoparticles were supported on nitrogen-doped carbon. Co/N-C-600 can converted vanillin into MMP with 99% yield in 8 h at 150 °C, 1 MPa H<sub>2</sub>.<sup>24</sup> Ga-doped Cu supported on H-nanozeolite-Y (Cu/HNZY) was fabricated by Verma et al and employed to catalyzing the HDO of vanillin. 99%

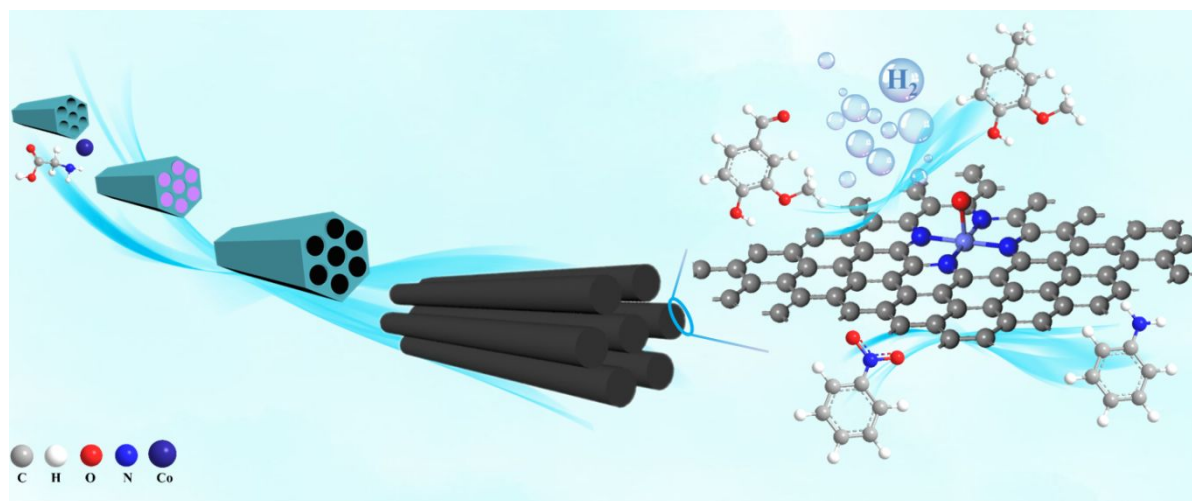
1  
2 selectivity was achieved with methanol as solvent after 2 h reaction at 160 °C.<sup>25</sup> Vanillin was  
3  
4 converted to MMP with 87% yield in 12 h at the condition of 150 °C, 2.5 MPa H<sub>2</sub> over Cu-Ni/CeO<sub>2</sub>-  
5  
6 SiO<sub>2</sub> catalyst.<sup>26</sup> ZnO/Co@N-CNT can also catalyze the HDO of vanillin, but the yield of MMP was  
7  
8 low (89.1%) and the dosage of metal was large.<sup>27</sup> Despite recent progress, the reported non-noble  
9  
10 metal-based catalysts still suffer one or more shortcomings, such as high catalyst loading, high H<sub>2</sub>  
11  
12 pressure, poor selectivity and long reaction time. Thus, exploring highly efficient non-noble metal-  
13  
14 based catalysts for the HDO of lignin-derived species still remains a challenge.  
15  
16

17  
18 Single atom catalysts (SACs), as a rising star in catalysis, have attracted broad attention since it  
19  
20 shows the merits of maximize atomic utilization, well-defined mononuclear structures and  
21  
22 remarkably promoted catalytic properties.<sup>28-30</sup> The SACs have already been employed in the field of  
23  
24 electrocatalysis (CO<sub>2</sub> reduction,<sup>31</sup> O<sub>2</sub> reduction,<sup>32</sup> H<sub>2</sub> reduction reaction<sup>33</sup>), photocatalysis (CO<sub>2</sub>  
25  
26 reduction<sup>34-35</sup> and H<sub>2</sub> evolution reduction<sup>36</sup>) and catalytic hydrogenation reaction (alkynes<sup>37</sup> and  
27  
28 styrene<sup>38</sup> hydrogenation, nitroarene hydrogenation<sup>39</sup>), oxidation reaction (benzene oxidation,<sup>40</sup>  
29  
30 glucose oxidation,<sup>41</sup> selective oxidation of alcohols<sup>42</sup> and C-H bonds<sup>43</sup>) and other coupling  
31  
32 reactions.<sup>44-45</sup> Thanks to the properties of higher metal loading and exposing more active sites on  
33  
34 the support surface of the obtained SACs, sacrificial hard template method received more attention  
35  
36 for the preparation of SACs compared with other thermal condensation strategies.<sup>46-49</sup> For example,  
37  
38 Xu et al.<sup>50</sup> employed Fe-phenanthroline as the precursor and SBA-15 as the hard template, after  
39  
40 calcined at 950 °C followed by alkali and acid leaching, the obtained Fe SAs/MC exhibited  
41  
42 excellent ORR activity and durability. Zhang and co-workers<sup>51</sup> fabricated single atom catalyst Ni-  
43  
44 N-C by employing Ni-phenanthroline as the precursor and MgO as the template, which was active  
45  
46 for hydrogenation of various unsaturated substrates and extraordinary durability for cellulose  
47  
48 conversion under harsh conditions. ISAS-Co/OPNC<sup>52</sup> and Co-N-C<sup>53</sup> were also fabricated by hard  
49  
50 template assistant method and exhibited outstanding catalytic performance for catalyzing reaction.  
51  
52  
53  
54  
55  
56

57  
58 Until now, only single atom Ru catalyst, Ru<sub>1</sub>/mpg-C<sub>3</sub>N<sub>4</sub><sup>54</sup>, was reported for the HDO of vanillin.  
59  
60 Considering the economic benefits and catalytic efficiency, non-noble metal SACs with improved

1  
2 catalytic activity and selectivity are highly desirable.

3  
4 In this paper, Co supported on nitrogen-doped carbon catalysts were fabricated with  
5  
6  $\text{Co}(\text{NO}_3)_2 \cdot 6\text{H}_2\text{O}$  and glycine as the precursor and three kinds of  $\text{SiO}_2$  (MCM-41, SBA-15 and FDU-  
7  
8 12) with different microstructure as the hard template, respectively. The impact of pore structure of  
9  
10 the templates on the dispersity of Co was investigated for the first time. The coordination of metal  
11  
12 with ligands as well as the introduction of hard template might increase the dispersion of metal and  
13  
14 endow the catalysts with more exposed active sites and high surface area, which might render the  
15  
16 catalysts with enhanced activity. After calcinated at  $800\text{ }^\circ\text{C}$  followed by alkali leaching, atomically  
17  
18 dispersed Co supported on porous nitrogen-doped carbon ( $\text{Co}_1@\text{NC}(\text{SBA})$ ) was obtained with  
19  
20 SBA-15 as the template (Scheme 1). The  $\text{Co}_1@\text{NC}(\text{SBA})$  was characterized by high-angle annular  
21  
22 dark field aberration-corrected scanning transmission electron microscopy (HAADF-STEM) and X-  
23  
24 ray absorption spectroscopy (XAS).  $\text{Co}_1@\text{NC}(\text{SBA})$  manifested outstanding catalytic performance  
25  
26 for the hydrodeoxygenation of lignin-derived species as well as the hydrogenation of series  
27  
28 nitroarenes.  
29  
30  
31  
32  
33



34  
35  
36  
37  
38  
39  
40  
41  
42  
43  
44  
45  
46  
47  
48  
49  
50  
51 **Scheme 1.** Schematic illustration for the formation of  $\text{Co}_1@\text{NC}(\text{SBA})$ .

## 52 53 **EXPERIMENTAL SECTION**

54  
55  
56 **Preparation of FDU-12.** The ordered porous silica FDU-12 was prepared according to the  
57  
58 reported method reported by Bao et al.<sup>55</sup> Briefly, 0.50 g of Pluronic F127, 0.60 g of (TMB) and 2.5  
59  
60 g of KCl were dissolved in 30 ml of 2 M HCl at  $15 \pm 0.1\text{ }^\circ\text{C}$ . After 2 h stirring, 2.08 g of tetraethyl

1  
2 orthosilicate (TEOS) was added to this solution. After stirring for 24 h at 15°C, the mixture was  
3  
4 transferred into an autoclave and heated at 100°C for 24 h. The as-made products were obtained by  
5  
6 filtration and dried at room temperature in air. For the high-temperature hydrothermal treatment,  
7  
8 0.50 g of as-made products was added to a solution of 30 ml 2 M HCl in an autoclave and the  
9  
10 mixture was heated at desired temperature for another 48 h. The obtained solid was calcinated at  
11  
12 550 °C for 4h (5 °C/min, N<sub>2</sub>) to remove the organic templates.  
13  
14

15  
16 **Preparation of Series Catalysts.** Co<sub>1</sub>@NC-(SBA) was fabricated by using a support-sacrificing  
17  
18 method. Briefly, 2 g SBA-15 and 2 g glycine were first dissolved in a solution of 100 mL water and  
19  
20 100 mL ethanol, then 0.85 mmol Co(NO<sub>3</sub>)<sub>2</sub>·6H<sub>2</sub>O in 10 mL water was mixed with the above  
21  
22 solution. The resulting pink suspension was refluxed at 80°C for 12 h followed by removing the  
23  
24 solvent via rotary evaporation at 70°C. The obtained powder was calcinated at 800°C for 2 h  
25  
26 (5 °C/min, N<sub>2</sub>) followed by etching SBA-15 template and Co nanoparticles with 6 M NaOH at 60°C  
27  
28 for 24 h.  
29  
30  
31

32  
33 For comparison, Co@NC-(FDU) and Co@NC-(MCM) were synthesized by the above method  
34  
35 except that SBA-15 was replaced by FDU-12 and MCM-41, respectively. Cu@NC-(SBA) and  
36  
37 Ni@NC-(SBA) and Fe@NC-(SBA) were prepared in the same way of Co<sub>1</sub>@NC-(SBA) except that  
38  
39 0.85 mmol Cu(NO<sub>3</sub>)<sub>2</sub>·4H<sub>2</sub>O, 0.85 mmol Ni(NO<sub>3</sub>)<sub>2</sub>·6H<sub>2</sub>O and 0.85 mmol Fe(NO<sub>3</sub>)<sub>3</sub>·9H<sub>2</sub>O were  
40  
41 added to replace Co(NO<sub>3</sub>)<sub>2</sub>·6H<sub>2</sub>O, respectively.  
42  
43

44  
45 Co@NC was prepared as follows: 2 g glycine were dissolved in a solution of 50 mL water and 50  
46  
47 mL ethanol, then 251 mg Co(NO<sub>3</sub>)<sub>2</sub>·6H<sub>2</sub>O in 10 mL water was mixed with the above solution. The  
48  
49 obtained pink solution was kept stirring for 6 h at room temperature followed by rotary evaporation  
50  
51 at 70 °C to remove the solvent. The pink powder was calcined at 800 °C for 2 h at a heating rate of  
52  
53 5 °C/min under the protection of N<sub>2</sub> and then cooled to room temperature naturally. The obtained  
54  
55 material was grinded into powder, named as Co@NC.  
56  
57

58  
59 **Procedure for the Hydrogenation Reaction.** The catalytic hydrogenation of lignin-derived  
60  
species was carried out in a 50 mL Teflon-lined autoclave. Typically, 0.5 mmol of substrate, 30 mg

1 of Co<sub>1</sub>@NC-(SBA) and 4 mL of water were added into the autoclave, which was purged with  
2 nitrogen gas and then purged with hydrogen for four times, respectively. The final H<sub>2</sub> pressure was  
3  
4  
5  
6 set at 1 MPa. The autoclave was heated to 140 °C for a certain time with stirring at 1000 rpm. Cold  
7  
8  
9 water was employed to cool down the autoclave quickly after the reaction finished. The products  
10  
11 were extracted by dichloromethane and analyzed by GC-MS. The catalyst was separated by  
12  
13 filtration and washed with ethanol, and then dried at 60°C for further use.  
14

15  
16 The hydrogenation of nitroarenes was carried out in a 50 mL Teflon-lined autoclave. Typically,  
17  
18 0.5 mmol of nitro-compound, 28 mg of Co<sub>1</sub>@NC-(SBA) and 4 mL of ethanol were added into the  
19  
20 autoclave which was purged with nitrogen gas and then purged with hydrogen for four times,  
21  
22 respectively. The final H<sub>2</sub> pressure was set at 1 MPa. The autoclave was heated to 90 °C for a  
23  
24 certain time with stirring at 1000 rpm. Finally, the products were analyzed by GC-MS. The catalyst  
25  
26 was separated by filtration and washed with ethanol, and then dried at 60 °C for further use.  
27  
28

## 29 RESULTS AND DISSCUSION

30  
31  
32 **Characterization of the Catalysts.** High resolution transmission electron microscope (HRTEM)  
33  
34 images showed that MCM-41, SBA-15 and FDU-12 with different pore size all exhibited ordered  
35  
36 pore structure (Figure 1, a-c) and the Barrett-Joyner-Halenda (BJH) median pore width of MCM-41,  
37  
38 SBA-15 and FDU-12 are 2.66, 11.10 and 17.20 nm, respectively (Table S1 and Figure 2a-b). The  
39  
40 Brunner-Emmet-Teller (BET) surface area of MCM-41, SBA-15 and FDU-12 were 1065, 619 and  
41  
42 475 m<sup>2</sup>/g, respectively (Table S1).  
43  
44

45  
46 When the templates were etched away, Co@NC-(MCM) fabricated with MCM-41 as the  
47  
48 template exhibited layered structure and no obvious pores can be observed (Figure 1d). Co<sub>1</sub>@NC-  
49  
50 (SBA) fabricated with SBA-15 as the template possessed an ordered porous structure (Figure 1e).  
51  
52 HRTEM image of Co@NC-(FDU) (Figure 1f) fabricated with FDU-12 as the template showed that  
53  
54 its pore structure was complementary to that of FDU-12, but the pores of Co@NC-(FDU) partly  
55  
56 collapsed. The BET surface area and pore size of the prepared catalysts were listed in Table S1 as  
57  
58 well. Co<sub>1</sub>@NC-(SBA) possessed largest BET surface area, pore size as well as pore volume. No  
59  
60

obvious cobalt particles were detected in the HRTEM images of the prepared catalysts, signifying the cobalt was anchored on the support with high dispersity. Besides, the X-ray diffraction (XRD) patterns of Co@NC-(MCM), Co<sub>1</sub>@NC-(SBA) and Co@NC-(FDU) only displayed a broad peak at  $2\theta = 24^\circ$ , corresponding to the (002) plane of graphitic carbon, no diffraction peak of Co was found, which further demonstrated the well dispersion of the cobalt sites (Figure S1). As for Co@NC prepared in the absence of a hard template, obvious cobalt particles were observed in the HRTEM image (Figure S2). XRD patterns of Co@NC showed distinct peaks at  $44.2^\circ$ ,  $51.5^\circ$ , and  $75.8^\circ$  (Figure S1), which correspond to the (111), (200) and (220) planes of metallic Co (JCPDS No. 15-0806), respectively.<sup>56</sup> The BET surface area, pore volume and pore size of Co@NC were 433 m<sup>2</sup>/g, 0.51 cm<sup>3</sup>/g and 2.25 nm, respectively (Table S1, entry 7).

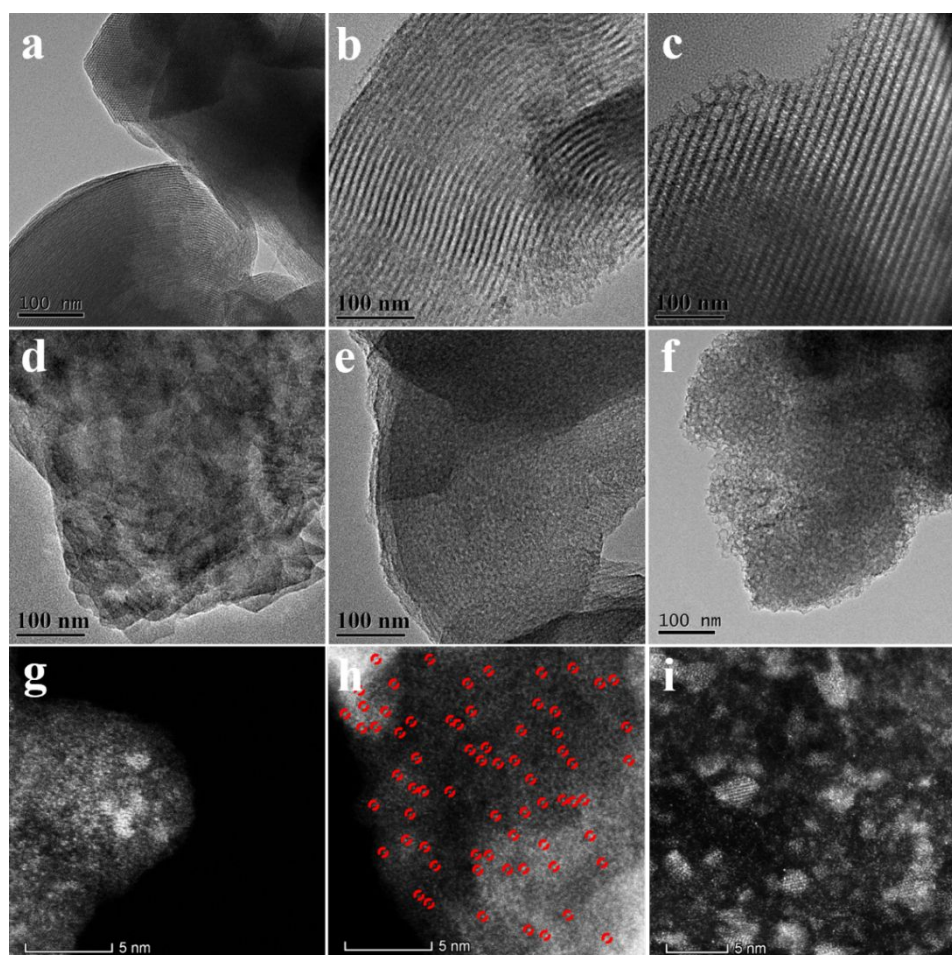


**Figure 1.** HRTEM images of MCM-41 (a), SBA-15 (b), FDU-12 (c), Co@NC-(MCM) (d), Co<sub>1</sub>@NC-(SBA) (e) and Co@NC-(FDU) (f). HAADF-STEM images of Co@NC-(MCM) (g), Co<sub>1</sub>@NC-(SBA) (h) and Co@NC-(FDU) (i).

Furthermore, high-angle annular dark-field scanning transmission electron microscopy (HAADF-STEM) was performed to characterize the dispersion of Co in the prepared catalysts. Both Co nanoparticles or clusters were observed in Co@NC-(MCM) (Figure 1g) and Co@NC-(FDU) (Figure 1i). As shown in Figure 1h, the observed brighter spots (highlighted by red circles) were identified as isolated Co single sites in Co<sub>1</sub>@NC-(SBA), and no cobalt cluster or nanoparticles was found in the sample.

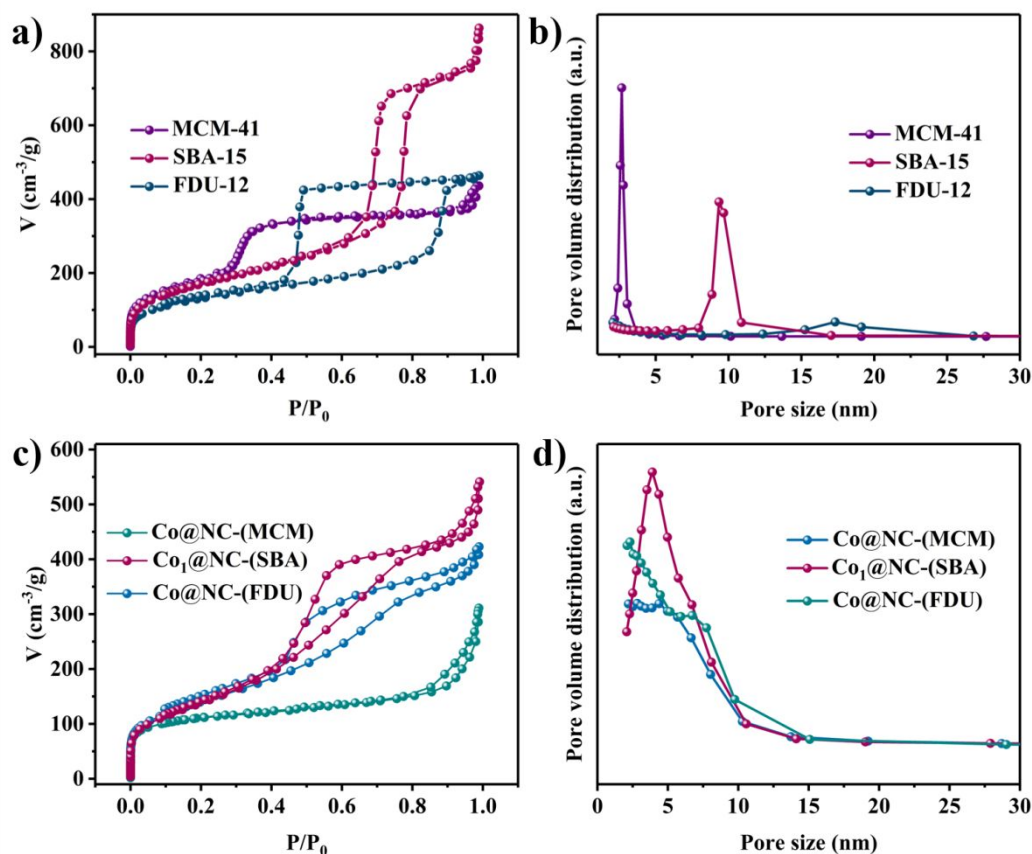


**Figure 2.** N<sub>2</sub> sorption isotherms (a) and BJH pore size distributions (b) of the employed SiO<sub>2</sub> templates. N<sub>2</sub> sorption isotherms (c) and BJH pore size distributions (d) of the series catalysts.

Based on the results of BET data, HRTEM and HAADF-STEM analysis, we can conclude that the SiO<sub>2</sub> templates with different pore structure directly affect the morphologies of the prepared catalysts and the dispersity of cobalt. For Co@NC-(MCM), Co(NO<sub>3</sub>)<sub>2</sub>·6H<sub>2</sub>O-glycine precursor was hard to transfer into the narrow pore of MCM-41, part of Co(NO<sub>3</sub>)<sub>2</sub>·6H<sub>2</sub>O-glycine precursor might adsorb on the surface of MCM-41, which led to the agglomeration of cobalt during the

1  
2 carbonization process. For FDU-12, although the  $\text{Co}(\text{NO}_3)_2 \cdot 6\text{H}_2\text{O}$ -glycine precursor can migrate  
3  
4 into the pores of FDU-12 easily, but the relatively large pores of FDU-12 did not have a strong  
5  
6 confinement and anchoring effect for Co complex during the pyrolysis process, resulting in the  
7  
8 formation of cobalt cluster. However, when SBA-15 was employed as the template, the  
9  
10  $\text{Co}(\text{NO}_3)_2 \cdot 6\text{H}_2\text{O}$ -glycine can be anchored in the pores of SBA-15 with moderate pore size via  
11  
12 hydrogen bonding interaction between the silicon hydroxyl in SBA-15 and the amino and carboxyl  
13  
14 groups in glycine. The confinement effect of SBA-15 with proper pore structure might prevent the  
15  
16 cobalt from aggregation during the carbonization process, guaranteeing the cobalt were  
17  
18 homogenously dispersed on the ordered nitrogen-doped carbon support after etching the template  
19  
20 away. The results of inductively coupled plasma atomic emission spectrometry (ICP-AES) can also  
21  
22 provide some evidence. The Co content in  $\text{Co}@NC\text{-}(MCM)$ ,  $\text{Co}_1@NC\text{-}(SBA)$  and  $\text{Co}@NC\text{-}(FDU)$   
23  
24 measured by ICP-AES were 5.3 wt%, 3.2 wt% and 3.8 wt%, respectively, where  $\text{Co}@NC\text{-}MCM$   
25  
26 showed highest content of Co as compared with  $\text{Co}@NC\text{-}SBA$  and  $\text{Co}@NC\text{-}FDU$ . The results  
27  
28 indicated the formation of more Co clusters in the catalysts when MCM-41 and FDU-12 were  
29  
30 employed as the templates. In addition, compared with MCM-41 and FDU-12, the unique three-  
31  
32 dimensional interconnected channel structure of SBA-15 would provide  $\text{Co}_1@NC\text{-}(SBA)$  with  
33  
34 much more ordered pores, leading to expose more catalytic active sites.  
35  
36  
37  
38  
39

40  
41 X-ray absorption near-edge structure (XANES) and extended X-ray absorption fine structure  
42  
43 (EXAFS) measurements were performed to analyze the electronic structure and coordination  
44  
45 environment of  $\text{Co}_1@NC\text{-}(SBA)$ . As shown in Figure 3a, the absorption edge position of  $\text{Co}_1@NC\text{-}$   
46  
47 (SBA) was located between that of  $\text{CoO}$  and  $\text{Co}_3\text{O}_4$ , suggesting that Co in the  $\text{Co}_1@NC\text{-}(SBA)$   
48  
49 carried a positive charge and the valence state of the Co was between  $\text{Co}^{2+}$  and  $\text{Co}^{3+}$ .<sup>57</sup> The Fourier-  
50  
51 transformed (FT)  $k_3$ -weighted EXAFS spectrum of  $\text{Co}_1@NC\text{-}(SBA)$  displayed a strong peak at 1.35  
52  
53 Å, corresponding to the Co-N or Co-C (Figure 3b), the absence of Co-Co coordination peak (2.18 Å)  
54  
55 further excluded the presence of metallic cobalt nanoparticles and confirmed that the Co in  
56  
57  $\text{Co}_1@NC\text{-}(SBA)$  sample was atomically dispersed.<sup>58</sup> Furthermore, the EXAFS wavelet transform  
58  
59  
60

(WT) plot (Figure 3c) of  $\text{Co}_1\text{@NC-(SBA)}$  showed only one intensity maximum at around  $k = 4 \text{ \AA}^{-1}$ , corresponding to the Co-N/C coordination. Compared with the WT plots of Co foil, CoO,  $\text{Co}_3\text{O}_4$  and CoPC (cobalt porphyrin) in Figure 3c, no WT maximum corresponding to Co-Co bonding can be observed in the R range from 1~3  $\text{\AA}$ .<sup>59-60</sup> Quantitative EXAFS fitting was then conducted to extract the structural parameters and obtain the precise coordination configuration of Co atom for  $\text{Co}_1\text{@NC-(SBA)}$ . The Co *K*-edges  $k^3\chi(k)$  oscillation curve in Figure 4d suggested the distinct local atomic arrangement of  $\text{Co}_1\text{@NC-(SBA)}$ , which was consistent with reported literature.<sup>61-62</sup> The best-fitting analyses (Figure 3e) clearly presented a main peak originating from Co-N/C first shell coordination. As shown in Table S2, the Co-N shell presented a coordination number of 5.3 at a distance of 1.91  $\text{\AA}$ . The error of the best-fitting results was within an acceptable error.

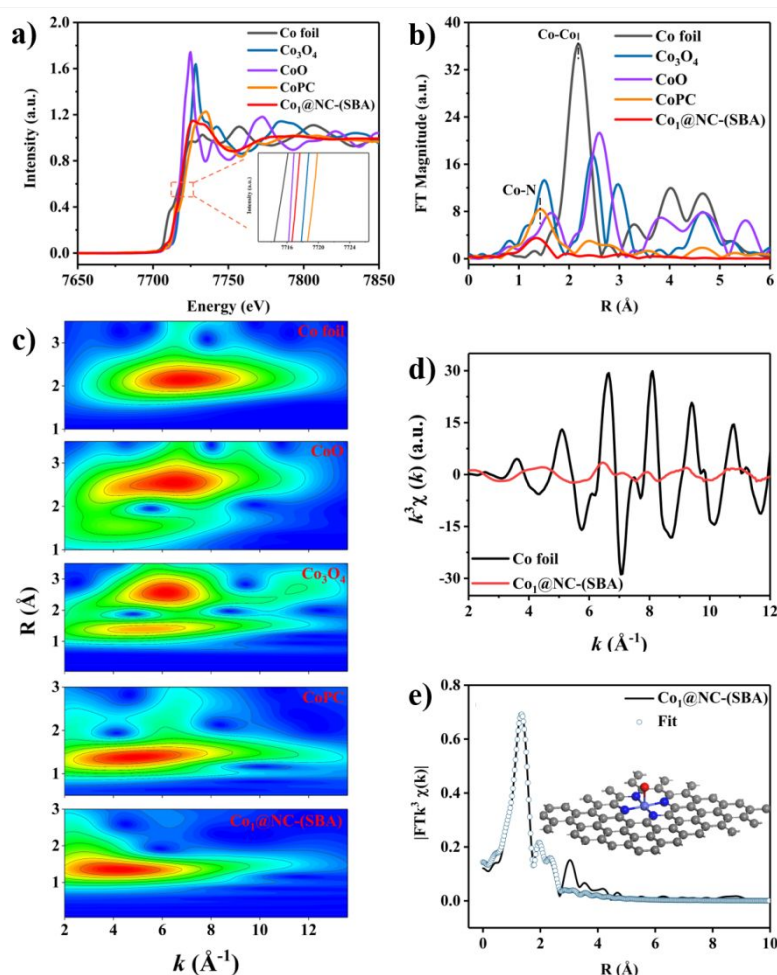


**Figure 3** XANES spectra (a) and Fourier transform (FT) EXAFS at the Co *K*-edge (b) of Co foil, CoO,  $\text{Co}_3\text{O}_4$ , CoPC and  $\text{Co}_1\text{@NC-(SBA)}$ . Wavelet transform (WT) for the  $k^3$ -weighted EXAFS signals of Co foil, CoO,  $\text{Co}_3\text{O}_4$ , CoPC and  $\text{Co}_1\text{@NC-(SBA)}$  (c). EXAFS spectra of  $\text{Co}_1\text{@NC-(SBA)}$  and Co foil at *K* space (d). The corresponding

EXAFS fitting curves of Co<sub>1</sub>@NC-(SBA) at *R* space (e), the inset of (e) is the schematic model of Co<sub>1</sub>@NC-(SBA), Co (pink), N (blue), O (red), C (grey).

The chemical states of Co and N in Co<sub>1</sub>@NC-(SBA) were also analyzed by X-ray photoelectron spectroscopy (XPS). As shown in Figure S3a, the binding energy (BE) of Co 2p<sub>3/2</sub> was located at 781.1 eV, corresponding to the Co-N<sub>x</sub> sites.<sup>63</sup> The N 1s XPS spectrum can be deconvoluted into three peaks at 398.3, 400.7 and 404.8 eV (Figure S3b), corresponding to pyridinic N, graphitic N and chemisorbed N-oxide, respectively.<sup>52</sup> The predominance of pyridinic N may coordinate with cobalt and served as an anchor for stabilizing the atomically dispersed cobalt sites more efficiently. The Co 2p<sub>3/2</sub> peaks of Co@NC-(MCM) (Figure S3c) with a BE of 779.6, 780.9 and 782.2 eV were attributed to Co<sub>3</sub>O<sub>4</sub><sup>64</sup> and the Co 2p<sub>3/2</sub> peak with a BE of 781.1 eV was attributed to Co-N<sub>x</sub>. The Co 2p<sub>3/2</sub> peaks of Co@NC-(FDU) (Figure S3d) with a BE of 780.0 and 782.1 eV can be assigned to CoO<sup>64</sup> and the Co 2p<sub>3/2</sub> peak with a BE of 781.1 eV was attributed to Co-N<sub>x</sub>. The content of Co-N<sub>x</sub> in Co@NC-(MCM) and Co@NC-(FDU) were about 6.6% and 14.4%, respectively, which is much lower than that in Co<sub>1</sub>@NC-(SBA). No metallic Co peak was found in the spectrum Co@NC-(MCM) and Co@NC-(FDU), the presence of cobalt oxide was due to the surface oxidation of Co nanoparticles or clusters in Co@NC-(MCM) and Co@NC-(FDU) during storage in the air.<sup>65</sup>

**Vanillin Hydrodeoxygenation.** The HDO of vanillin was selected as a model substrate to examine the catalytic activity of the series catalysts. The catalytic conditions including different catalysts, reaction temperature, initial H<sub>2</sub> pressure and solvent were optimized. The catalysts fabricated with different microstructure and degrees of Co dispersity exhibited distinguishing catalytic performance for the HDO of vanillin (Table 1). No conversion was observed with Co@NC contained large Co nanoparticles as catalyst (Table 1, entry 1), which was fabricated by directly carbonization of Co(NO<sub>3</sub>)<sub>2</sub>·6H<sub>2</sub>O-glycine complex complex without a template. 20.3% yield of MMP was obtained in 3 h when the reaction was performed with Co@NC-(MCM) as catalyst, the yield was only increased to 25.3% when the reaction time was extended to 6 h (Table 1, entries 2-3). For Co@NC-(FDU) catalyst, 32.6% and 57.6% yield of MMP were achieved after 3 h and 6 h

reaction, respectively (Table 1, entries 5-6). The results revealed that the cobalt in the form of nanoparticles or clusters displayed a relatively poor catalytic activity toward the HDO of vanillin. To our delight, vanillin can be transformed to MMP with 99.2% yield in H<sub>2</sub>O-MeOH (1:1, v/v) over Co<sub>1</sub>@NC-(SBA) at 140 °C, 1 MPa H<sub>2</sub> within 3 h (Table 1, entry 4). According to the results of XPS, the content of Co-N<sub>x</sub> in Co<sub>1</sub>@NC-(SBA) is much higher than that in Co@NC-(MCM) and Co@NC-(FDU), which further demonstrated the Co-N<sub>x</sub> sites were the active sites for the HDO of vanillin. We also prepared Fe@NC-(SBA), Ni@NC-(SBA) and Cu@NC-(SBA) to investigate the effect of the metal type on the catalytic performance (Table 1, entries 7-9), only Fe@NC-(SBA) was active for the HDO of vanillin, 7.5% yield of MMP was achieved in 3 h.

**Table 1.** HDO catalytic performance of vanillin <sup>a</sup>

Entry	Catalysts	Time (h)	Conv. (%)	MMP Yield (%)
1	Co@NC	3	0	0
2	Co@NC-(MCM)	3	25.7	20.3
3	Co@NC-(MCM)	6	31.6	25.3
4	Co <sub>1</sub> @NC-(SBA)	3	100	99.2
5	Co@NC-(FDU)	3	43.2	32.6
6	Co@NC-(FDU)	6	88.9	57.6
7	Fe@NC-(SBA)	3	8.2	7.5
8	Ni@NC-(SBA)	3	0	0
9	Cu@NC-(SBA)	3	0	0

<sup>a</sup> Reaction conditions: 0.5 mmol vanillin, 3.25 mol% Co, 1 MPa H<sub>2</sub>, 140 °C, 2 mL H<sub>2</sub>O, 2 mL MeOH.

The reaction pathway of the HDO of vanillin over Co<sub>1</sub>@NC-(SBA) in H<sub>2</sub>O-MeOH (1:1, v/v) was further investigated (Figure 4a). In the initial reaction stage, the reaction was carried out with a mild increase in the conversion of vanillin and the yield of MMP. The yield of HMP increased until 30 min and then decreased slowly. 68.1% conversion of vanillin and 53% yield of MMP were achieved within 1 h. When the reaction time prolonged to 3 h, vanillin was completely converted and the

selectivity for MMP was 99.2%. It should be mentioned that the formation of 4-hydroxymethyl-2-methoxyphenol (HMP) and 2-methoxy-4-(methoxymethyl) phenol (DMP) were relatively low (<10%) in the whole reaction process (Figure 4a, S4).

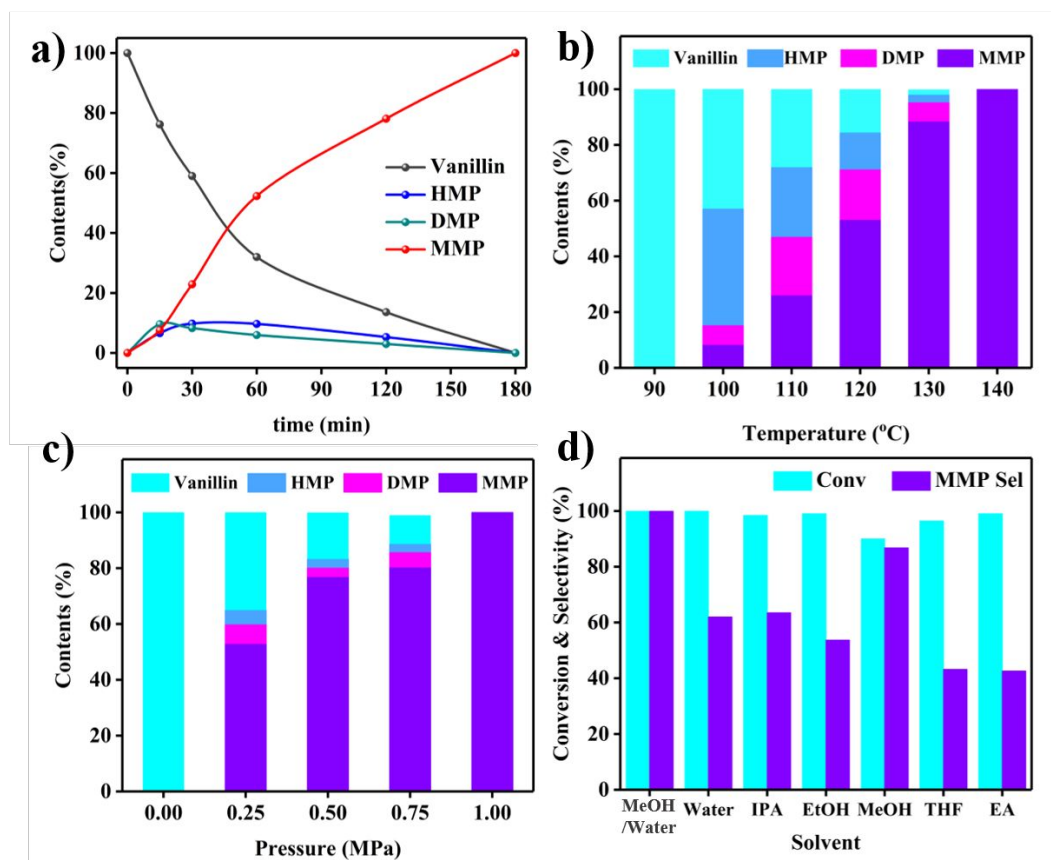
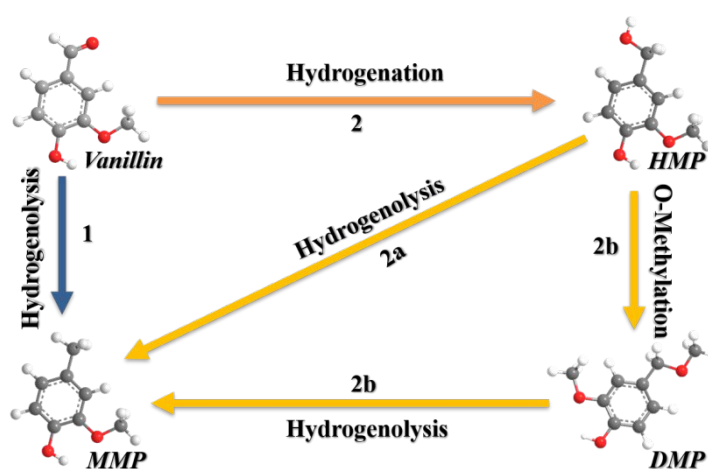


**Figure 4.** Optimization of the reaction conditions for HDO reaction of vanillin over  $\text{Co}_1\text{@NC-(SBA)}$ . Reaction conditions: 0.5 mmol vanillin, 30 mg  $\text{Co}_1\text{@NC-(SBA)}$  (3.25 mol% Co): Effect of reaction time. 1 MPa  $\text{H}_2$ , 2 mL  $\text{H}_2\text{O}$ , 2 mL MeOH, 140 °C (a). Effect of reaction temperature. 1 MPa  $\text{H}_2$ , 2 mL  $\text{H}_2\text{O}$ , 2 mL MeOH, 3 h (b). Effect of  $\text{H}_2$  pressure. 2 mL  $\text{H}_2\text{O}$ , 2 mL MeOH, 140 °C, 3 h (c). Effect of the type of solvent. 1 MPa  $\text{H}_2$ , 4 mL solvent, 140 °C, 3 h (d).

The reaction temperature played a significant role in the conversion of vanillin and selectivity of MMP. As shown in Figure 4b, the HDO of vanillin was not occurred when the temperature was lower than 100 °C. HMP and DMP were formed when the reaction temperature was between 100 °C and 140 °C. The increment of temperature led to the improvement of vanillin conversion and MMP selectivity. Vanillin was completely converted to MMP when the reaction was executed at 140 °C. The impact of initial  $\text{H}_2$  pressure on the hydrodeoxygenation of vanillin was also investigated at 140 °C for 3 h. As shown in Figure 4c, increasing the initial  $\text{H}_2$  pressure can

1  
2 accelerate the conversion of vanillin and the yield of MMP with the H<sub>2</sub> pressure increase from 0.25  
3  
4 MPa to 1 MPa, which can be ascribed to the capacity for adsorption of H<sub>2</sub>. Complete conversion of  
5  
6 vanillin and excellent MMP yield of 99.2% was achieved with 1 MPa H<sub>2</sub> pressure.  
7

8  
9 The influence of reaction solvent for the HDO of vanillin over Co<sub>1</sub>@NC-(SBA) catalyst was  
10 further conducted (Figure 4d). Among the various solvent examined, high conversion of vanillin  
11 was achieved in the common solvents including water, isopropanol (IPA), ethanol, methanol,  
12  
13 tetrahydrofuran (THF) and ethyl acetate (EA). When water was employed as the solvent, 99%  
14  
15 conversion was achieved in 2 h, no HMP and other by-products were detected, whereas the mass  
16  
17 balance of MMP was only 64%. Besides, when HMP was selected the substance, HMP was  
18  
19 completely converted in 1 h with water as the solvent and the MMP yield was 52%. According to  
20  
21 the previous reports, the loss in mass balance was mainly caused by the polymerization of the  
22  
23 substrates and the oligomer was formed during the polycondensation process.<sup>20, 66</sup> When methanol  
24  
25 was employed as the solvent, the mass balance was 100% when the reaction time prolonged to 3 h,  
26  
27 but the conversion of vanillin and the yield of MMP were 90% and 86.8%, respectively. Vanillin  
28  
29 was completely converted to MMP with 99.2% yield in 3 h when methanol-H<sub>2</sub>O (1:1, v/v) was used  
30  
31 as the solvent. It can be concluded from above results that the selectivity of MMP was mainly  
32  
33 affected by the reaction temperature, reaction time and solvent rather than H<sub>2</sub> pressure.  
34  
35  
36  
37  
38  
39  
40  
41



58 **Scheme 2.** Reaction pathways of hydrodeoxygenation of vanillin.  
59  
60

1  
2 For comparison, control experiment for hydrogenolysis of HMP was conducted and the results  
3 were shown in Figure S5. Nearly 100% conversion of HMP was achieved in the first 40 min. As the  
4 reaction conducted further, the main initial product, DMP, was gradually converted to MMP via  
5 hydrogenolysis. These results indicated that the transformation of HMP to MMP was much easier  
6 than that of vanillin to MMP. So, when vanillin was used as substrate, the content of HMP and  
7 DMP during the whole reaction was low (Figure 4a).  
8  
9  
10  
11  
12  
13  
14

15 To further reveal the reaction mechanism, the HDO of the mixture of vanillin and HMP was also  
16 conducted under the optimal reaction conditions. When the mole ratio of vanillin and HMP was 1:1  
17 (0.25 mmol vanillin and 0.25 mmol HMP) and 9:1, the conversion of vanillin after 2 h reaction was  
18 12% and 18%, respectively, which were much lower than that with only vanillin as substrate; while  
19 HMP was converted completely. The results demonstrated that the presence of HMP may inhibit the  
20 conversion of vanillin to some extent.  
21  
22  
23  
24  
25  
26  
27  
28  
29

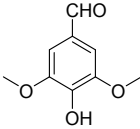
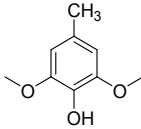
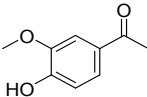
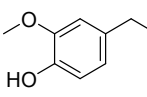
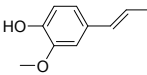
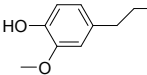
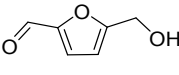
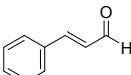
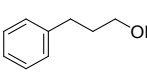
30 The kinetic studies were further conducted to obtain more insights into the conversion of vanillin  
31 to MMP. The calculated activation energy of the hydrogenation of vanillin to HMP and the  
32 hydrogenolysis of HMP to MMP based on the slope value of Arrhenius plots (Figure S6) were  
33 130.2 kJ/mol and 86.5 kJ/mol, respectively. The activation energy of the HMP hydrogenolysis  
34 reaction was lower than that of vanillin hydrogenation, which further suggested that the  
35 hydrogenolysis of HMP was more easily than the hydrogenation of vanillin.  
36  
37  
38  
39  
40  
41  
42  
43

44 The possible reaction pathways of the HDO of vanillin were proposed in Scheme 2. Previously, it  
45 has been reported that two reaction pathways existed for the transformation of a carbonyl group into  
46 a methyl group in aqueous solution, MMP can be obtained by the direct hydrogenolysis of vanillin  
47 (Scheme 2, path 1) or the hydrogenation of vanillin into HMP, and subsequent hydrogenolysis of  
48 HMP into MMP (Scheme 2, path 2a).<sup>17</sup> As for the HDO of vanillin in methanol media, it was  
49 reported that the reaction can also be proceeded via the path 2a; moreover, the presence of DMP  
50 revealed that another pathway existed,<sup>25</sup> in which DMP was formed by the *o*-methylation of HMP,  
51 followed by the hydrogenolysis of DMP to produce MMP (Scheme 2, path 2b). On the basis of the  
52  
53  
54  
55  
56  
57  
58  
59  
60

time course reaction data and the kinetic studies, we proposed that MMP was mainly obtained via the hydrogenation-hydrogenolysis route (Scheme 2, path 2).

For other lignin-derived species, *o*-vanillin, syringaldehyde and acetovanillone can be completely converted to corresponding HDO products on Co<sub>1</sub>@NC-(SBA) under the optimized conditions (Table 2, entries 1-3). After 3 h reaction, isoeugenol was transformed into 2-methoxy-4-propylphenol with 99% yield (Table 2, entry 4). 5-hydroxymethylfurfural (HMF) can also be transformed to 2, 5-dimethylfuran (DMF) with 99% conversion and 82.6% selectivity at mild conditions (Table 2, entry 5). Besides, cinnamyl alcohol was converted to phenylpropanol at mild condition with 91.4% yield (Table 2, entry 6).

**Table 2.** The hydrogenation reactions of serious lignin-derived species over Co<sub>1</sub>@NC-(SBA)<sup>a</sup>

Entry	Substrates	Products	Conv. (%)	Sel. (%)
1			99	99
2			99	99
3			99	99
4			99	99
5 <sup>b</sup>			99	82.6
6 <sup>c</sup>			99	91.4

<sup>a</sup> Reaction conditions: 0.5 mmol substrate, 30 mg Co<sub>1</sub>@NC-(SBA) (3.25 mol% Co), 2 mL H<sub>2</sub>O, 2 mL MeOH, 140 °C, 1 MPa H<sub>2</sub>, 3 h. <sup>b</sup> 2 MPa H<sub>2</sub>, 4 mL EtOH, 180 °C, 4 h, <sup>c</sup> 2 MPa H<sub>2</sub>, 4 mL EtOH, 120 °C, 2 h.

**Density Functional Theory (DFT) Calculations.** DFT calculations were further applied to uncover the intrinsic influence of Co electronic structure on the catalytic activity of CoN<sub>x</sub>. Three

1  
2 typical Co-N<sub>x</sub> models with different coordination numbers, including Co-N<sub>4</sub> (a CoN<sub>4</sub> moiety  
3 embedded in graphene layer), Co-N<sub>4</sub>O and Co-N<sub>5</sub> (possible structures when the coordination  
4 number is five) (Figure S7),<sup>67-68</sup> were built to conduct the calculation by using first principle method.  
5  
6  
7  
8  
9 The computational details were provided in the Supporting Information (Table S3-S4, Figure S8-  
10 S12). For comparison, Co particles (Co<sub>12</sub> cluster) were used to simulate the Co@NC catalyst.  
11  
12 According to the optimized structures, compared with the Co-N bond length (1.86 Å) in CoN<sub>4</sub> sites,  
13 the Co-N bond length (1.89 Å) in the Co-N<sub>5</sub> or Co-N<sub>4</sub>O site was closest to that of EXAFS fitting  
14 results (1.91 Å). The adsorption energies of the main species (H<sub>2</sub>, H\*, vanillin, HMP, DMP and  
15 MMP) involved in the reaction process on the four possible active sites, Co-N<sub>5</sub>, Co-N<sub>4</sub>O, CoN<sub>4</sub> and  
16 Co particles, were calculated and the results were shown in Table S3. Calculation results revealed  
17 that the adsorption energies of the main species on Co<sub>12</sub> were too large and led to the catalyst  
18 deactivation. The conclusion was consistent with the experimental results. In addition, DFT  
19 calculations also confirmed that the adsorption energy of HMP on CoN<sub>4</sub> sites was lower than that of  
20 vanillin (Table S3), suggesting that HMP is more easily adsorbed and then activated (Figure S8).  
21  
22 The result was consistent with the experimental result: in detail the transformation of HMP to MMP  
23 was easier than that of vanillin to HMP. So, the reaction pathway most probably undergo a  
24 hydrogenation-hydrogenolysis route.  
25  
26  
27  
28  
29  
30  
31  
32  
33  
34  
35  
36  
37  
38  
39  
40

41 The adsorption energies of H<sub>2</sub> on the three active sites were low (-0.14 eV~ -0.38 eV) (Table S3,  
42 entry 2). The adsorption distances between Co and H<sub>2</sub> on the active sites were about 3.0 Å (Table  
43 S4, entry 1). The bond lengths of H<sub>2</sub> molecule and the adsorbed H<sub>2</sub>\* on Co N<sub>4</sub>O or CoN<sub>5</sub> had no  
44 evident difference (Table S4, entry 2), which indicated that the interaction between hydrogen  
45 molecule and CoN<sub>4</sub>O or CoN<sub>5</sub> was weak, and there was no obvious chemical interaction between  
46 them, so the adsorption of H<sub>2</sub> on CoN<sub>4</sub>O or CoN<sub>5</sub> belonged to physically adsorption.<sup>69</sup> The bond  
47 length of hydrogen molecule adsorbed on CoN<sub>4</sub> sites was 0.799 Å (Figure S9), which was larger  
48 than that of free hydrogen molecule (0.751 Å). This result indicated that the Co<sub>1</sub>@NC-(SBA)  
49 catalyst could indeed activate hydrogen molecule. However, the activation of H<sub>2</sub> on the model  
50  
51  
52  
53  
54  
55  
56  
57  
58  
59  
60

1  
2 catalyst was not easier than that on metal cobalt nanoparticle catalyst because the system energy  
3  
4 increases slightly (about 0.11 eV) in contrast to the energy of free catalyst and hydrogen. However,  
5  
6 in the presence of vanillin, homolytic cleavage of H-H bond of the activated hydrogen occurred  
7  
8 (Figure S10). And one active H\* is captured by carbonyl oxygen of vanillin and the other H\* is left  
9  
10 on the cobalt site of CoN<sub>4</sub> sites (Figure S10, step 1). The energy in this step has a slight increase  
11  
12 (0.1 eV), which can be achieved easily at high reaction temperature.  
13  
14

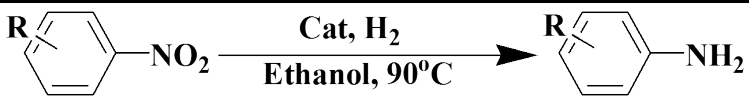
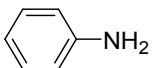
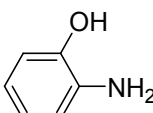
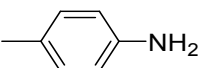
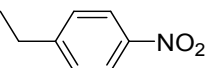
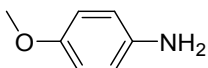
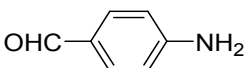
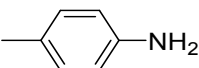
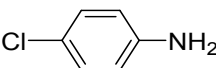
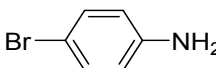
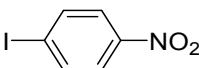
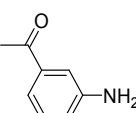
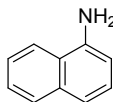
15  
16 According to the results reported in the literatures, although the adsorption energy of H<sub>2</sub> on the  
17  
18 active sites was low, the spontaneous dissociation of H<sub>2</sub> over the metal sites can still occur  
19  
20 efficiently.<sup>69-70</sup> The dissociated H can be adsorbed on Co atoms and the nearby O or N atoms to  
21  
22 form Co-H, O-H and N-H species,<sup>70</sup> respectively. The *d* band center model is a good descriptor of  
23  
24 the adsorbate-metal interaction.<sup>71</sup> The greater the energy difference between the *d*-band center of  
25  
26 the active sites and the corresponding Fermi level ( $E_f = 0$ ), the weaker the adsorption of the  
27  
28 adsorbate on the active sites. In order to discuss the role of *d*-orbital electron involved in the  
29  
30 reactions, the occupied *d*-band center of the three active sites were calculated (Table S4, entry 4).  
31  
32 The results suggested that the adsorption energies of the active H were relatively low (Table S4,  
33  
34 entry 5) and the adsorption of the active H on the active sites was weak, which facilitated the  
35  
36 desorption of H from the catalyst sites and enhanced the catalytic reaction.  
37  
38  
39

40  
41 The Bader charge analysis of the Co-N<sub>5</sub>, Co-N<sub>4</sub>O and CoN<sub>4</sub> sites were shown in Table S5.  
42  
43 According to the calculation data, the charge of Co atom was greatly affected by the outer  
44  
45 coordination atom. Because of the large electronegativity of O and N atoms, the charge of Co atom  
46  
47 increased from 0.83 e<sup>-</sup> on Co-N<sub>4</sub> sites to above 1.0 e<sup>-</sup> on Co-N<sub>4</sub>O sites and Co-N<sub>5</sub> sites. Vanillin was  
48  
49 easier to be adsorbed and H\* radicals were easier to be desorbed on the Co-N<sub>4</sub>O sites and Co-N<sub>5</sub>  
50  
51 sites because the increased positive charge of Co. The Bader charge analysis also approved the  
52  
53 results of adsorption energy.  
54  
55

56  
57 **Hydrogenation Reaction of Nitroarenes.** To verify the application potential of Co<sub>1</sub>@NC-(SBA),  
58  
59 the hydrogenation reaction of nitro-compounds to corresponding aromatic amines was further  
60

investigated since they play an important part in the manufacture of dyes, pharmaceuticals, pigments as well as their intermediates.<sup>72-74</sup> The hydrogenation of *p*-nitrochlorobenzene was employed as the model reaction to optimize the reaction conditions. As shown in the Table S6, both the activity and selectivity were significantly affected by the H<sub>2</sub> pressure, reaction temperature, time and solvent.

**Table 3.** Substrates scope of the hydrogenation reaction of nitro-compounds. <sup>a</sup>

			
1	2	3	4
 1.5 h, 99%	 1.5 h, 99%	 1.5 h, 99%	 2 h, 99%
5	6	7	8
 2 h, 99%	 2 h, 99%	 2 h, 99%	 2 h, 99%
9 <sup>b</sup>	10	11	12
 2 h, 99%	 1 h, 99%	 2 h, 99%	 2 h, 99%
13	14	15	16
 2 h, 99%	 2 h, 99%	 2 h, 99%	 2 h, 99%

<sup>a</sup> Reaction conditions: 0.5 mmol substrate, 28 mg Co<sub>1</sub>@NC-(SBA), 4 mL ethanol, 90 °C, 1 MPa initial H<sub>2</sub>. <sup>b</sup> 140 °C.

The hydrogenation of series nitroarenes were carried out under the optimized conditions (90 °C,

1  
2 1 MPa H<sub>2</sub>, ethanol as the solvent, 0.5 mmol substrate, 28 mg Co<sub>1</sub>@NC-(SBA)) and the results were  
3  
4 summarized in Table 3. Most of the functionalized nitroarenes can be converted to corresponding  
5  
6 aromatic amines within 2 h. The series nitroarenes with electron donating groups such as *p*-amino,  
7  
8 *p*-hydroxyl, *o*-hydroxyl, *p*-methyl, *p*-ethyl and *p*-nitroanisole can be transformed to the  
9  
10 corresponding amines with 100% yield within 2 h (Table 3, entries 2-7). Nitro-compounds with  
11  
12 electron absorption groups such as *p*-formyl, *p*-halogen, *p*-acetyl, *m*-acetyl, *p*-cyano and 1-  
13  
14 nitronaphthalene achieved 99% conversion and 99% selectivity too (Table 3, entries 8, 10-16).  
15  
16 Furthermore, the aldehyde group on *p*-nitrobenzaldehyde was transformed to methyl as well when  
17  
18 the reaction was conducted at 140 °C (Table 3, entry 9), the results were in good consistence with  
19  
20 the HDO reaction of vanillin.  
21  
22  
23

24  
25 One of the greatest concerns regarding the use of SACs for liquid-phase reactions is its stability.  
26  
27 Generally, the hydrogenation of *p*-nitrochlorobenzene was conducted to verify the reusability of  
28  
29 Co<sub>1</sub>@NC-(SBA). As shown in Figure S13a, after ten continuous runs, the conversion and  
30  
31 selectivity of *p*-nitrochlorobenzene kept at 94% and 94%, respectively. HAADF-STEM image of  
32  
33 the recycled Co<sub>1</sub>@NC-(SBA) displayed that the cobalt was still atomically dispersed and no cluster  
34  
35 was observed (Figure S13b), indicating the outstanding reusability and high stability of the Co-N<sub>x</sub>  
36  
37 bonds.  
38  
39

40  
41 In addition, we summarized the materials recently reported for catalyzing the HDO of vanillin  
42  
43 and hydrogenation of nitro-compounds, the results were listed in Table S7 and Table S8,  
44  
45 respectively. The catalytic performance for the HDO of vanillin of Co<sub>1</sub>@NC-(SBA) was  
46  
47 comparable or even superior to some of the previously reported noble metal catalysts (Table S7,  
48  
49 entries 1-4) or higher than the reported non-noble catalysts (Table S7, entries 6-16). Besides, the  
50  
51 catalytic performance for the hydrogenation of nitro-compounds on Co<sub>1</sub>@NC-(SBA) was  
52  
53 comparable or superior to the reported non-noble catalysts as well (Table S8, 7-12). Those results  
54  
55 further demonstrated the highly catalytic activity of Co<sub>1</sub>@NC-(SBA) in the heterogeneous  
56  
57 hydrogenation reaction.  
58  
59  
60

## CONCLUSIONS

A hard-template sacrificial strategy was developed to prepare SACs Co catalyst  $\text{Co}_1@NC-(\text{SBA})$  by employing  $\text{Co}(\text{NO}_3)_2 \cdot 6\text{H}_2\text{O}$ -glycine complex as the precursor and SBA-15 as the template. For comparison, the catalysts fabricated by MCM-41 and FDU-12 presented obviously difference of Co dispersity. Among all the prepared catalysts, atomically dispersed Co catalyst  $\text{Co}_1@NC-(\text{SBA})$  exhibited the best catalytic activity, which was not only active for the hydrodeoxygenation of lignin-derived species with excellent yield, but also exhibited highly catalytic activity for the hydrogenation of various nitroarenes under mild conditions.  $\text{Co}_1@NC-(\text{SBA})$  also manifested good reusability for the heterogeneous hydrogenation reaction. The highly catalytic activity and good stability of  $\text{Co}_1@NC-(\text{SBA})$  were attributed to the atomical dispersity of Co and its  $\text{CoN}_4\text{O}$  structure.

## ASSOCIATED CONTENT

### Supporting Information

The Supporting Information is available free of charge on the ACS Publications website at DOI:

Chemicals and reagents, apparatus, DFT Calculation details, XRD and XPS patterns of the series catalysts, HRTEM image of  $\text{Co}@NC$ , catalyst recycle and HAADF-STEM of reused  $\text{Co}_1@NC-(\text{SBA})$ , surface area and pore size of the series  $\text{SiO}_2$  templates and catalysts, EXAFS data fitting results of  $\text{Co}_1@NC-(\text{SBA})$ , optimization of the hydrogenation of nitro-compounds, summary of reported literatures for the HDO of vanillin and hydrogenation of nitro-compounds

## AUTHOR INFORMATION

† These authors contributed equally to this work.

Corresponding Author

\* Chun Wang, Phone: +86-312-7528291. Fax: +86-312-7528292. E-mail: wangchun@hebau.edu.cn, chunwang69@126.com.

Shutao Gao, E-mail: gaoshutao@hebau.edu.cn

Yuqing Qiao, E-mail: qiaoyq@ysu.edu.cn.

1  
2 Yongjun Gao, E-mail: [yjgao@hbu.edu.cn](mailto:yjgao@hbu.edu.cn).

3  
4 **ORCID**

5  
6 Chun Wang:

7  
8  
9 Yongjun Gao:

10  
11 **Notes**

12  
13 The authors declare no competing financial interest.

14  
15 **ACKNOWLEDGMENTS**

16  
17  
18 Financial supports from National Natural Science Foundation of China (31671930, 21773053),  
19  
20 Natural Science Foundation of Hebei Province (B2020204003, B2019204023, B2018204145,  
21  
22 B2016204131, B2015204003) and the One Hundred Talent Project of Hebei Province  
23  
24 (E2016100015) are acknowledged. The DFT calculation was carried out on TianHe-2 at LvLiang  
25  
26 Cloud Computing Center of China.  
27  
28  
29  
30  
31

32  
33 **REFERENCES**

- 34  
35 (1) Singh, A. K.; Jang, S.; Kim, J. Y.; Sharma, S.; Basavaraju, K. C.; Kim, M.-G.; Kim, K.-R.; Lee, J. S.;  
36 Lee, H. H.; Kim, D.-P., One-Pot Defunctionalization of Lignin-Derived Compounds by Dual-Functional  
37 Pd<sub>50</sub>Ag<sub>50</sub>/Fe<sub>3</sub>O<sub>4</sub>/N-Rgo Catalyst. *ACS Catal.* **2015**, *5*, 6964-6972.  
38 (2) Zhang, F.; Jin, Y.; Fu, Y.; Zhong, Y.; Zhu, W.; Ibrahim, A. A.; El-Shall, M. S., Palladium  
39 Nanoparticles Incorporated within Sulfonic Acid-Functionalized Mil-101(Cr) for Efficient Catalytic  
40 Conversion of Vanillin. *J Mater. Chem. A* **2015**, *3*, 17008-17015.  
41 (3) Hao, P.; Schwartz, D. K.; Medlin, J. W., Effect of Surface Hydrophobicity of Pd/Al<sub>2</sub>O<sub>3</sub> on Vanillin  
42 Hydrodeoxygenation in a Water/Oil System. *ACS Catal.* **2018**, *8*, 11165-11173.  
43 (4) Wang, Q.; Feng, J.; Zheng, L.; Wang, B.; Bi, R.; He, Y.; Liu, H.; Li, D., Interfacial Structure-  
44 Determined Reaction Pathway and Selectivity for 5-(Hydroxymethyl)Furfural Hydrogenation over Cu-Based  
45 Catalysts. *ACS Catal.* **2020**, *10*, 1353-1365.  
46 (5) Huber, G. W.; Iborra, S.; Corma, A., Synthesis of Transportation Fuels from Biomass: Chemistry,  
47 Catalysts, and Engineering. *Chem. Rev.* **2006**, *106*, 4044-4098.  
48 (6) Saidi, M.; Samimi, F.; Karimipourfard, D.; Nimmanwudipong, T.; Gates, B. C.; Rahimpour, M. R.,  
49 Upgrading of Lignin-Derived Bio-Oils by Catalytic Hydrodeoxygenation. *Energ. Environ. Sci.* **2014**, *7*, 103-  
50 129.  
51 (7) Zacher, A. H.; Olarte, M. V.; Santosa, D. M.; Elliott, D. C.; Jones, S. B., A Review and Perspective of  
52 Recent Bio-Oil Hydrotreating Research. *Green Chem.* **2014**, *16*, 491-515.  
53 (8) Chheda, J. N.; Huber, G. W.; Dumesic, J. A., Liquid-Phase Catalytic Processing of Biomass-Derived  
54 Oxygenated Hydrocarbons to Fuels and Chemicals. *Angew. Chem. Int. Ed.* **2007**, *46*, 7164-83.  
55 (9) Yang, J.; Williams, C. L.; Ramasubramaniam, A.; Dauenhauer, P. J., Aqueous-Phase  
56 Hydrodeoxygenation of Highly Oxygenated Aromatics on Platinum. *Green Chem.* **2014**, *16*, 675-682.  
57 (10) Fache, M.; Boutevin, B.; Caillol, S., Vanillin Production from Lignin and Its Use as a Renewable  
58 Chemical. *ACS Sustain. Chem. Eng.* **2015**, *4*, 6379-6401.  
59  
60

- (11) Yang, X.; Liang, Y.; Zhao, X.; Song, Y.; Hu, L.; Wang, X.; Wang, Z.; Qiu, J., Au/Cnts Catalyst for Highly Selective Hydrodeoxygenation of Vanillin at the Water/Oil Interface. *RSC Advances* **2014**, *4*, 31932-31936.
- (12) Zhu, L.; Jiang, Y.; Zheng, J.; Zhang, N.; Yu, C.; Li, Y.; Pao, C. W.; Chen, J. L.; Jin, C.; Lee, J. F.; Zhong, C. J.; Chen, B. H., Ultrafine Nanoparticle-Supported Ru Nanoclusters with Ultrahigh Catalytic Activity. *Small* **2015**, *11*, 4385-4393.
- (13) Yang, X.; Liang, Y.; Cheng, Y.; Song, W.; Wang, X.; Wang, Z.; Qiu, J., Hydrodeoxygenation of Vanillin over Carbon Nanotube-Supported Ru Catalysts Assembled at the Interfaces of Emulsion Droplets. *Catal. Commun.* **2014**, *47*, 28-31.
- (14) Zhu, Z.; Tan, H.; Wang, J.; Yu, S.; Zhou, K., Hydrodeoxygenation of Vanillin as a Bio-Oil Model over Carbonaceous Microspheres-Supported Pd Catalysts in the Aqueous Phase and Pickering Emulsions. *Green Chem.* **2014**, *16*, 2636-2643.
- (15) Chen, Y.-Z.; Cai, G.; Wang, Y.; Xu, Q.; Yu, S.-H.; Jiang, H.-L., Palladium Nanoparticles Stabilized with N-Doped Porous Carbons Derived from Metal-Organic Frameworks for Selective Catalysis in Biofuel Upgrade: The Role of Catalyst Wettability. *Green Chem.* **2016**, *18*, 1212-1217.
- (16) Zhang, F.; Zheng, S.; Xiao, Q.; Zhong, Y.; Zhu, W.; Lin, A.; Samy El-Shall, M., Synergetic Catalysis of Palladium Nanoparticles Encaged within Amine-Functionalized UiO-66 in the Hydrodeoxygenation of Vanillin in Water. *Green Chem.* **2016**, *18*, 2900-2908.
- (17) Aijaz, A.; Zhu, Q.-L.; Tsumori, N.; Akita, T.; Xu, Q., Surfactant-Free Pd Nanoparticles Immobilized to a Metal-Organic Framework with Size- and Location-Dependent Catalytic Selectivity. *Chem. Commun.* **2015**, *51*, 2577-2580.
- (18) Zhang, J.; Sun, K.; Li, D.; Deng, T.; Lu, G.; Cai, C., Pd-Ni Bimetallic Nanoparticles Supported on Active Carbon as an Efficient Catalyst for Hydrodeoxygenation of Aldehydes. *Appl. Catal. A: Gen.* **2019**, *569*, 190-195.
- (19) Jongerius, A. L.; Jastrzebski, R.; Bruijninx, P. C. A.; Weckhuysen, B. M., Como Sulfide-Catalyzed Hydrodeoxygenation of Lignin Model Compounds: An Extended Reaction Network for the Conversion of Monomeric and Dimeric Substrates. *J. Catal.* **2012**, *285*, 315-323.
- (20) He, L.; Qin, Y.; Lou, H.; Chen, P., Highly Dispersed Molybdenum Carbide Nanoparticles Supported on Activated Carbon as an Efficient Catalyst for the Hydrodeoxygenation of Vanillin. *RSC Advances* **2015**, *5*, 43141-43147.
- (21) Petitjean, L.; Gagne, R.; Beach, E. S.; Xiao, D.; Anastas, P. T., Highly Selective Hydrogenation and Hydrogenolysis Using a Copper-Doped Porous Metal Oxide Catalyst. *Green Chem.* **2016**, *18*, 150-156.
- (22) Nie, R.; Yang, H.; Zhang, H.; Yu, X.; Lu, X.; Zhou, D.; Xia, Q., Mild-Temperature Hydrodeoxygenation of Vanillin over Porous Nitrogen-Doped Carbon Black Supported Nickel Nanoparticles. *Green Chem.* **2017**, *19*, 3126-3134.
- (23) Fan, R.; Chen, C.; Han, M.; Gong, W.; Zhang, H.; Zhang, Y.; Zhao, H.; Wang, G., Highly Dispersed Copper Nanoparticles Supported on Activated Carbon as an Efficient Catalyst for Selective Reduction of Vanillin. *Small* **2018**, *14*, e1801953.
- (24) Jiang, L.; Zhou, P.; Liao, C.; Zhang, Z.; Jin, S., Cobalt Nanoparticles Supported on Nitrogen-Doped Carbon: An Effective Non-Noble Metal Catalyst for the Upgrade of Biofuels. *ChemSusChem* **2018**, *11*, 959-964.
- (25) Verma, D.; Insyani, R.; Cahyadi, H. S.; Park, J.; Kim, S. M.; Cho, J. M.; Bae, J. W.; Kim, J., Ga-Doped Cu/H-Nanozeolite-Y Catalyst for Selective Hydrogenation and Hydrodeoxygenation of Lignin-Derived Chemicals. *Green Chem.* **2018**, *20*, 3253-3270.
- (26) Mukherjee, D.; Singuru, R.; Venkataswamy, P.; Damma, D.; Reddy, B. M., Ceria Promoted Cu-Ni/SiO<sub>2</sub> Catalyst for Selective Hydrodeoxygenation of Vanillin. *ACS Omega* **2019**, *4*, 4770-4778.
- (27) Ranaware, V.; Verma, D.; Insyani, R.; Riaz, A.; Kim, S. M.; Kim, J., Highly-Efficient and Magnetically-Separable Zn/Co@N-Cnts Catalyst for Hydrodeoxygenation of Lignin and Its Derived Species under Mild Conditions. *Green Chem.* **2019**, *21*, 1021-1042.
- (28) Zhang, L.; Liu, X.; Zhou, X.; Gao, S.; Shang, N.; Feng, C.; Wang, C., Ultrafine Pd Nanoparticles Anchored on Nitrogen-Doping Carbon for Boosting Catalytic Transfer Hydrogenation of Nitroarenes. *ACS Omega* **2018**, *3*, 10843-10850.
- (29) Zhang, L.; Ren, Y.; Liu, W.; Wang, A.; Zhang, T., Single-Atom Catalyst: A Rising Star for Green Synthesis of Fine Chemicals. *Natl. Sci. Rev.* **2018**, *5*, 653-672.
- (30) Jiang, K.; Siahrostami, S.; Zheng, T.; Hu, Y.; Hwang, S.; Stavitski, E.; Peng, Y.; Dynes, J.; Gangisetty, M.; Su, D.; Attenkofer, K.; Wang, H., Isolated Ni Single Atoms in Graphene Nanosheets for High-Performance CO<sub>2</sub> Reduction. *Energ. Environ. Sci.* **2018**, *11*, 893-903.

- (31) Cheng, Y.; Zhao, S.; Johannessen, B.; Veder, J. P.; Saunders, M.; Rowles, M. R.; Cheng, M.; Liu, C.; Chisholm, M. F.; De Marco, R.; Cheng, H. M.; Yang, S. Z.; Jiang, S. P., Atomically Dispersed Transition Metals on Carbon Nanotubes with Ultrahigh Loading for Selective Electrochemical Carbon Dioxide Reduction. *Adv. Mater.* **2018**, *30*, e1706287.
- (32) Holby, E. F.; Wu, G.; Zelenay, P.; Taylor, C. D., Structure of Fe-N<sub>x</sub>-C Defects in Oxygen Reduction Reaction Catalysts from First-Principles Modeling. *J. Phys. Chem. C* **2014**, *118*, 14388-14393.
- (33) Qiu, H. J.; Ito, Y.; Cong, W.; Tan, Y.; Liu, P.; Hirata, A.; Fujita, T.; Tang, Z.; Chen, M., Nanoporous Graphene with Single-Atom Nickel Dopants: An Efficient and Stable Catalyst for Electrochemical Hydrogen Production. *Angew. Chem. Int. Ed. Engl.* **2015**, *54*, 14237-14241.
- (34) Gao, G.; Jiao, Y.; Waclawik, E. R.; Du, A., Single Atom (Pd/Pt) Supported on Graphitic Carbon Nitride as an Efficient Photocatalyst for Visible-Light Reduction of Carbon Dioxide. *J. Am. Chem. Soc.* **2016**, *138*, 6292-6297.
- (35) Cheng, Y.; Zhao, S.; Li, H.; He, S.; Veder, J.-P.; Johannessen, B.; Xiao, J.; Lu, S.; Pan, J.; Chisholm, M. F.; Yang, S.-Z.; Liu, C.; Chen, J. G.; Jiang, S. P., Unsaturated Edge-Anchored Ni Single Atoms on Porous Microwave Exfoliated Graphene Oxide for Electrochemical CO<sub>2</sub>. *Appl. Catal., B: Environ.* **2019**, *243*, 294-303.
- (36) Li, X.; Bi, W.; Zhang, L.; Tao, S.; Chu, W.; Zhang, Q.; Luo, Y.; Wu, C.; Xie, Y., Single-Atom Pt as Co-Catalyst for Enhanced Photocatalytic H<sub>2</sub> Evolution. *Adv. Mater.* **2016**, *28*, 2427-2431.
- (37) Vile, G.; Albani, D.; Nachttegaal, M.; Chen, Z.; Dontsova, D.; Antonietti, M.; Lopez, N.; Perez-Ramirez, J., A Stable Single-Site Palladium Catalyst for Hydrogenations. *Angew. Chem. Int. Ed. Engl.* **2015**, *54*, 11265-11269.
- (38) Yan, H.; Cheng, H.; Yi, H.; Lin, Y.; Yao, T.; Wang, C.; Li, J.; Wei, S.; Lu, J., Single-Atom Pd<sub>1</sub>/Graphene Catalyst Achieved by Atomic Layer Deposition: Remarkable Performance in Selective Hydrogenation of 1,3-Butadiene. *J. Am. Chem. Soc.* **2015**, *137*, 10484-10487.
- (39) Zhang, B.; Asakura, H.; Zhang, J.; Zhang, J.; De, S.; Yan, N., Stabilizing a Platinum<sub>1</sub> Single-Atom Catalyst on Supported Phosphomolybdic Acid without Compromising Hydrogenation Activity. *Angew. Chem. Int. Ed.* **2016**, *55*, 8319-8323.
- (40) Deng, D.; Chen, X.; Yu, L.; Wu, X.; Liu, Q.; Liu, Y.; Yang, H.; Tian, H.; Hu, Y.; Du, P., A Single Iron Site Confined in a Graphene Matrix for the Catalytic Oxidation of Benzene at Room Temperature. *Sci. Adv.* **2015**, *1*, e1500462.
- (41) Zhang, H.; Watanabe, T.; Okumura, M.; Haruta, M.; Toshima, N., Catalytically Highly Active Top Gold Atom on Palladium Nanocluster. *Nat. Mater.* **2011**, *11*, 49-52.
- (42) Li, M.; Wu, S.; Yang, X.; Hu, J.; Peng, L.; Bai, L.; Huo, Q.; Guan, J., Highly Efficient Single Atom Cobalt Catalyst for Selective Oxidation of Alcohols. *Appl. Catal. A: Gen.* **2017**, *543*, 61-66.
- (43) Liu, W.; Zhang, L.; Liu, X.; Liu, X.; Yang, X.; Miao, S.; Wang, W.; Wang, A.; Zhang, T., Discriminating Catalytically Active Fe<sub>n</sub> Species of Atomically Dispersed Fe-N-C Catalyst for Selective Oxidation of the C-H Bond. *J. Am. Chem. Soc.* **2017**, *139*, 10790-10798.
- (44) Chen, Z.; Vorobyeva, E.; Mitchell, S.; Fako, E.; Ortuno, M. A.; Lopez, N.; Collins, S. M.; Midgley, P. A.; Richard, S.; Vile, G.; Perez-Ramirez, J., A Heterogeneous Single-Atom Palladium Catalyst Surpassing Homogeneous Systems for Suzuki Coupling. *Nat. Nanotechnol.* **2018**, *13*, 702-707.
- (45) Zhang, L.; Wang, A.; Miller, J. T.; Liu, X.; Yang, X.; Wang, W.; Li, L.; Huang, Y.; Mou, C.-Y.; Zhang, T., Efficient and Durable Au Alloyed Pd Single-Atom Catalyst for the Ullmann Reaction of Aryl Chlorides in Water. *ACS Catal.* **2014**, *4*, 1546-1553.
- (46) Malonzo, C. D.; Shaker, S. M.; Ren, L.; Prinslow, S. D.; Platero-Prats, A. E.; Gallington, L. C.; Borycz, J.; Thompson, A. B.; Wang, T. C.; Farha, O. K.; Hupp, J. T.; Lu, C. C.; Chapman, K. W.; Myers, J. C.; Penn, R. L.; Gagliardi, L.; Tsapatsis, M.; Stein, A., Thermal Stabilization of Metal-Organic Framework-Derived Single-Site Catalytic Clusters through Nanocasting. *J. Am. Chem. Soc.* **2016**, *138*, 2739-2748.
- (47) Zhang, H.; Wei, J.; Dong, J.; Liu, G.; Shi, L.; An, P.; Zhao, G.; Kong, J.; Wang, X.; Meng, X.; Zhang, J.; Ye, J., Efficient Visible-Light-Driven Carbon Dioxide Reduction by a Single-Atom Implanted Metal-Organic Framework. *Angew. Chem. Int. Ed. Engl.* **2016**, *55*, 14310-14314.
- (48) Zhang, T.; Zhang, D.; Han, X.; Dong, T.; Guo, X.; Song, C.; Si, R.; Liu, W.; Liu, Y.; Zhao, Z., Preassembly Strategy to Fabricate Porous Hollow Carbonitride Spheres Inlaid with Single Cu-N<sub>3</sub> Sites for Selective Oxidation of Benzene to Phenol. *J. Am. Chem. Soc.* **2018**, *140*, 16936-16940.
- (49) Han, Y.; Wang, Y. G.; Chen, W.; Xu, R.; Zheng, L.; Zhang, J.; Luo, J.; Shen, R. A.; Zhu, Y.; Cheong, W. C.; Chen, C.; Peng, Q.; Wang, D.; Li, Y., Hollow N-Doped Carbon Spheres with Isolated Cobalt Single Atomic Sites: Superior Electrocatalysts for Oxygen Reduction. *J. Am. Chem. Soc.* **2017**, *139*, 17269-17272.

- (50) Yang, Z.; Yuan, C.; Xu, A., Confined Pyrolysis within a Nanochannel to Form a Highly Efficient Single Iron Site Catalyst for Zn-Air Batteries. *ACS Energy Lett.* **2018**, *3*, 2383-2389.
- (51) Liu, W.; Chen, Y.; Qi, H.; Zhang, L.; Yan, W.; Liu, X.; Yang, X.; Miao, S.; Wang, W.; Liu, C.; Wang, A.; Li, J.; Zhang, T., A Durable Nickel Single-Atom Catalyst for Hydrogenation Reactions and Cellulose Valorization under Harsh Conditions. *Angew. Chem. Int. Ed. Engl.* **2018**, *57*, 7071-7075.
- (52) Han, Y.; Wang, Z.; Xu, R.; Zhang, W.; Chen, W.; Zheng, L.; Zhang, J.; Luo, J.; Wu, K.; Zhu, Y.; Chen, C.; Peng, Q.; Liu, Q.; Hu, P.; Wang, D.; Li, Y., Ordered Porous Nitrogen-Doped Carbon Matrix with Atomically Dispersed Cobalt Sites as an Efficient Catalyst for Dehydrogenation and Transfer Hydrogenation of N-Heterocycles. *Angew. Chem. Int. Ed. Engl.* **2018**, *57*, 11262-11266.
- (53) Liu, W.; Zhang, L.; Yan, W.; Liu, X.; Yang, X.; Miao, S.; Wang, W.; Wang, A.; Zhang, T., Single-Atom Dispersed Co-N-C Catalyst: Structure Identification and Performance for Hydrogenative Coupling of Nitroarenes. *Chem Sci* **2016**, *7*, 5758-5764.
- (54) Tian, S.; Wang, Z.; Gong, W.; Chen, W.; Feng, Q.; Xu, Q.; Chen, C.; Chen, C.; Peng, Q.; Gu, L.; Zhao, H.; Hu, P.; Wang, D.; Li, Y., Temperature-Controlled Selectivity of Hydrogenation and Hydrodeoxygenation in the Conversion of Biomass Molecule by the Ru<sub>1</sub>/Mpg-C<sub>3</sub>N<sub>4</sub> Catalyst. *J. Am. Chem. Soc.* **2018**, *140*, 11161-11164.
- (55) Fan, J.; Yu, C.; Lei, J.; Zhang, Q.; Li, T.; Tu, B.; Zhou, W.; Zhao, D., Low-Temperature Strategy to Synthesize Highly Ordered Mesoporous Silicas with Very Large Pores. *J. Am. Chem. Soc.* **2005**, *127*, 10794-10795.
- (56) Wu, Z. Y.; Xu, S. L.; Yan, Q. Q.; Chen, Z. Q.; Ding, Y. W.; Li, C.; Liang, H. W.; Yu, S. H., Transition Metal-Assisted Carbonization of Small Organic Molecules toward Functional Carbon Materials. *Sci. Adv.* **2018**, *4*, eaat0788.
- (57) Zhu, Y.; Sun, W.; Luo, J.; Chen, W.; Cao, T.; Zheng, L.; Dong, J.; Zhang, J.; Zhang, M.; Han, Y.; Chen, C.; Peng, Q.; Wang, D.; Li, Y., A Cocoon Silk Chemistry Strategy to Ultrathin N-Doped Carbon Nanosheet with Metal Single-Site Catalysts. *Nat. Commun.* **2018**, *9*, 3861.
- (58) Yin, P.; Yao, T.; Wu, Y.; Zheng, L.; Lin, Y.; Liu, W.; Ju, H.; Zhu, J.; Hong, X.; Deng, Z.; Zhou, G.; Wei, S.; Li, Y., Single Cobalt Atoms with Precise N-Coordination as Superior Oxygen Reduction Reaction Catalysts. *Angew. Chem. Int. Ed. Engl.* **2016**, *55*, 10800-10805.
- (59) Pan, Y.; Lin, R.; Chen, Y.; Liu, S.; Zhu, W.; Cao, X.; Chen, W.; Wu, K.; Cheong, W. C.; Wang, Y.; Zheng, L.; Luo, J.; Lin, Y.; Liu, Y.; Liu, C.; Li, J.; Lu, Q.; Chen, X.; Wang, D.; Peng, Q.; Chen, C.; Li, Y., Design of Single-Atom Co-N<sub>5</sub> Catalytic Site: A Robust Electrocatalyst for CO<sub>2</sub> Reduction with Nearly 100% Co Selectivity and Remarkable Stability. *J. Am. Chem. Soc.* **2018**, *140*, 4218-4221.
- (60) Zhu, Y.; Sun, W.; Chen, W.; Cao, T.; Xiong, Y.; Luo, J.; Dong, J.; Zheng, L.; Zhang, J.; Wang, X.; Chen, C.; Peng, Q.; Wang, D.; Li, Y., Scale-up Biomass Pathway to Cobalt Single-Site Catalysts Anchored on N-Doped Porous Carbon Nanobelt with Ultrahigh Surface Area. *Adv. Funct. Mater.* **2018**, *28*, 1802167.
- (61) Meng, T.; Qin, J.; Xu, D.; Cao, M., Atomic Heterointerface-Induced Local Charge Distribution and Enhanced Water Adsorption Behavior in Cobalt Phosphide Electrocatalyst for Self-Powered Highly Efficient Overall Water Splitting. *ACS Appl. Mater. Inter.* **2019**, *11*, 9023-9032.
- (62) Meng, T.; Hao, Y.; Zheng, L.; Cao, M., Organophosphoric Acid-Derived Cop Quantum Dots@S,N-Codoped Graphite Carbon as a Trifunctional Electrocatalyst for Overall Water Splitting and Zn-Air Batteries. *Nanoscale* **2018**, *10*, 14613-14626.
- (63) Zhou, P.; Jiang, L.; Wang, F.; Deng, K.; Lv, K.; Zhang, Z., High Performance of a Cobalt-Nitrogen Complex for the Reduction and Reductive Coupling of Nitro Compounds into Amines and Their Derivatives. *Sci. Adv.* **2017**, *3*, e1601945.
- (64) Biesinger, M. C.; Payne, B. P.; Grosvenor, A. P.; Lau, L. W. M.; Gerson, A. R.; Smart, R. S. C., Resolving Surface Chemical States in Xps Analysis of First Row Transition Metals, Oxides and Hydroxides: Cr, Mn, Fe, Co and Ni. *Appl. Surf. Sci.* **2011**, *257*, 2717-2730.
- (65) Zheng, B.; Wang, J.; Wang, F.-B.; Xia, X.-H., Low-Loading Cobalt Coupled with Nitrogen-Doped Porous Graphene as Excellent Electrocatalyst for Oxygen Reduction Reaction. *J Mater. Chem. A* **2014**, *2*, 9079-9084.
- (66) Sulman, A.; Mäki-Arvela, P.; Bomont, L.; Fedorov, V.; Alda-Onggar, M.; Smeds, A.; Hemming, J.; Russo, V.; Wärnå, J.; Kåldström, M.; Murzin, D. Y., Vanillin Hydrodeoxygenation: Kinetic Modelling and Solvent Effect. *Catal. Lett.* **2018**, *148*, 2856-2868.
- (67) Lai, Q.; Zheng, L.; Liang, Y.; He, J.; Zhao, J.; Chen, J., Metal-Organic-Framework-Derived Fe-N/C Electrocatalyst with Five-Coordinated Fe-N<sub>x</sub> Sites for Advanced Oxygen Reduction in Acid Media. *ACS Catal.* **2017**, *7*, 1655-1663.

- 1  
2 (68) Han, Y.; Wang, Y.; Xu, R.; Chen, W.; Zheng, L.; Han, A.; Zhu, Y.; Zhang, J.; Zhang, H.; Luo, J.;  
3 Chen, C.; Peng, Q.; Wang, D.; Li, Y., Electronic Structure Engineering to Boost Oxygen Reduction Activity  
4 by Controlling the Coordination of the Central Metal. *Energ. Environ. Sci.* **2018**, *11*, 2348-2352.
- 5 (69) Li, K.; Liu, H.; Zhang, R.; Ling, L.; Wang, B., Interaction between Bimetal Cluster Ni<sub>2</sub>Co<sub>2</sub> and Mgo  
6 and Its Effect on H Adsorption and H<sub>2</sub> Dissociation: A Dft Study. *Appl. Surf. Sci.* **2016**, *390*, 7-16.
- 7 (70) Wang, L.; Zhang, W.; Wang, S.; Gao, Z.; Luo, Z.; Wang, X.; Zeng, R.; Li, A.; Li, H.; Wang, M.;  
8 Zheng, X.; Zhu, J.; Zhang, W.; Ma, C.; Si, R.; Zeng, J., Atomic-Level Insights in Optimizing Reaction Paths  
9 for Hydroformylation Reaction over Rh/Co<sub>o</sub> Single-Atom Catalyst. *Nat Commun* **2016**, *7*, 14036.
- 10 (71) Chen, Z.; Song, Y.; Cai, J.; Zheng, X.; Han, D.; Wu, Y.; Zang, Y.; Niu, S.; Liu, Y.; Zhu, J.; Liu, X.;  
11 Wang, G., Tailoring the D-Band Centers Enables Co<sub>4</sub> N Nanosheets to Be Highly Active for Hydrogen  
12 Evolution Catalysis. *Angew. Chem. Int. Ed. Engl.* **2018**, *57*, 5076-5080.
- 13 (72) Zhang, L.; Wang, J.; Shang, N.; Gao, S.; Gao, Y.; Wang, C., Ultra Dispersed Cobalt Anchored on  
14 Nitrogen-Doping Ordered Porous Carbon as an Efficient Transfer Hydrogenation Catalyst. *Appl. Surf. Sci.*  
15 **2019**, *491*, 544-552.
- 16 (73) Cheng, S.; Shang, N.; Zhou, X.; Feng, C.; Gao, S.; Wang, C.; Wang, Z., High Catalytic Activity of a  
17 Bimetallic Agpd Alloy Supported on Uio-66 Derived Porous Carbon for Transfer Hydrogenation of  
18 Nitroarenes Using Formic Acid-Formate as the Hydrogen Source. *New J. Chem.* **2017**, *41*, 9857-9865.
- 19 (74) Yang, F.; Chi, C.; Wang, C.; Wang, Y.; Li, Y., High Graphite N Content in Nitrogen-Doped  
20 Graphene as an Efficient Metal-Free Catalyst for Reduction of Nitroarenes in Water. *Green Chem.* **2016**, *18*,  
21 4254-4262.  
22  
23  
24  
25  
26  
27  
28  
29  
30  
31  
32  
33  
34  
35  
36  
37  
38  
39  
40  
41  
42  
43  
44  
45  
46  
47  
48  
49  
50  
51  
52  
53  
54  
55  
56  
57  
58  
59  
60

## TOC Graphic

